Northumbria Research Link

Citation: Zahertar, Shahrzad, Yalcinkaya, Arda and Torun, Hamdi (2015) Rectangular split-ring resonators with single-split and two-splits under different excitations at microwave frequencies. AIP Advances, 5 (11). p. 117220. ISSN 2158-3226

Published by: American Institute of Physics

URL: https://doi.org/10.1063/1.4935910 <https://doi.org/10.1063/1.4935910>

This version was downloaded from Northumbria Research Link: http://nrl.northumbria.ac.uk/id/eprint/33032/

Northumbria University has developed Northumbria Research Link (NRL) to enable users to access the University's research output. Copyright © and moral rights for items on NRL are retained by the individual author(s) and/or other copyright owners. Single copies of full items can be reproduced, displayed or performed, and given to third parties in any format or medium for personal research or study, educational, or not-for-profit purposes without prior permission or charge, provided the authors, title and full bibliographic details are given, as well as a hyperlink and/or URL to the original metadata page. The content must not be changed in any way. Full items must not be sold commercially in any format or medium without formal permission of the copyright holder. The full policy is available online: http://nrl.northumbria.ac.uk/policies.html

This document may differ from the final, published version of the research and has been made available online in accordance with publisher policies. To read and/or cite from the published version of the research, please visit the publisher's website (a subscription may be required.)

Northumbria University NEWCASTLE

University Library

Rectangular split-ring resonators with single-split and two-splits under different excitations at microwave frequencies

S. Zahertar, A. D. Yalcinkaya, and H. Torun

Citation: AIP Advances **5**, 117220 (2015);
View online: https://doi.org/10.1063/1.4935910
View Table of Contents: http://aip.scitation.org/toc/adv/5/11
Published by the American Institute of Physics

Articles you may be interested in

Split-ring resonator for use in magnetic resonance from 200–2000 MHz
Review of Scientific Instruments **52**, 213 (1998); 10.1063/1.1136574

Electric coupling to the magnetic resonance of split ring resonators
Applied Physics Letters **84**, 2943 (2004); 10.1063/1.1695439

Electrically small split ring resonator antennas
Journal of Applied Physics **101**, 083104 (2007); 10.1063/1.2722232

Electromagnetic resonances in individual and coupled split-ring resonators
Journal of Applied Physics **92**, 2929 (2002); 10.1063/1.1497452

Complex permittivity measurement using metamaterial split ring resonators
Journal of Applied Physics **121**, 054101 (2017); 10.1063/1.4975111

Calculation and measurement of bianisotropy in a split ring resonator metamaterial
Journal of Applied Physics **100**, 024507 (2006); 10.1063/1.2218033

Rectangular split-ring resonators with single-split and two-splits under different excitations at microwave frequencies

S. Zahertar,[1] A. D. Yalcinkaya,[1,2] and H. Torun[1,2]
[1]*Department of Electrical and Electronics Engineering, Bogazici University, Bebek 34342 Istanbul, Turkey*
[2]*Center for Life Sciences and Technologies, Bogazici University, Kandilli 34684 Istanbul, Turkey*

(Received 21 September 2015; accepted 4 November 2015; published online 11 November 2015)

In this work, transmission characteristics of rectangular split-ring resonators with single-split and two-splits are analyzed at microwave frequencies. The resonators are coupled with monopole antennas for excitation. The scattering parameters of the devices are investigated under different polarizations of E and H fields. The magnetic resonances induced by E and H fields are identified and the differences in the behavior of the resonators due to orientations of the fields are explained based on simulation and experimental results. The addition of the second split of the device is investigated considering different configurations of the excitation vectors. It is demonstrated that the single-split and the two-splits resonators exhibit identical transmission characteristics for a certain excitation configuration as verified with simulations and experiments. The presented resonators can effectively function as frequency selective media for varying excitation conditions. © *2015 Author(s). All article content, except where otherwise noted, is licensed under a Creative Commons Attribution 3.0 Unported License.* [http://dx.doi.org/10.1063/1.4935910]

I. INTRODUCTION

Metamaterials are artificially engineered structures that exhibit unique properties such as having negative values of permittivity and permeability simultaneously in a specific frequency band, resulting in negative values of index of refraction.[1–3] These structures usually operate at resonance and their resonant frequencies depend highly on the geometry of the structure. Metamaterials have been demonstrated in a wide range of frequencies, spanning from GHz to optical frequencies[4] for various applications such as cloaking,[5,6] super lenses,[7,8] sub-diffraction focusing,[9] perfect absorption,[10] and biosensing.[11–16] Split-ring resonators (SRR) are among the basic building blocks to realize metamaterials.[17] SRRs are thin metallic rings or square loops with a split on top of a dielectric substrate. SRRs are one of the first metamaterial-based microwave resonators whose geometries are smaller than the wavelength of exciting electromagnetic waves.[18]

So far, different designs have been introduced in the field of metamaterials and the most conventional ones are circular and rectangular split-ring resonators. These are investigated regarding different performance parameters such as sensitivity for sensing applications. Rectangular designs are capable of providing higher sensitivity when they are employed for sensing applications.[19] Furthermore, rectangular resonators are more suitable for miniaturization and dense packing as compared to circular structures.[19] In addition, some modifications have been introduced to conventional designs such as fabricating multi-gap rectangular or circular split-ring resonators. It is shown that additional gaps to the structures prevent magnetic resonance due to the induced current by the electric field.[20–22] In addition, the resonant frequency usually shifts towards higher values.

In this paper, we present rectangular split-ring resonators that operate at microwave frequencies. We investigate resonators with a single-split and two splits. Our findings indicate that these resonators can exhibit the same frequency response under specific circumstances, which is counter-intuitive. In section II, we explain the structure and present the design of the device. We present the

 ©Author(s) 2015

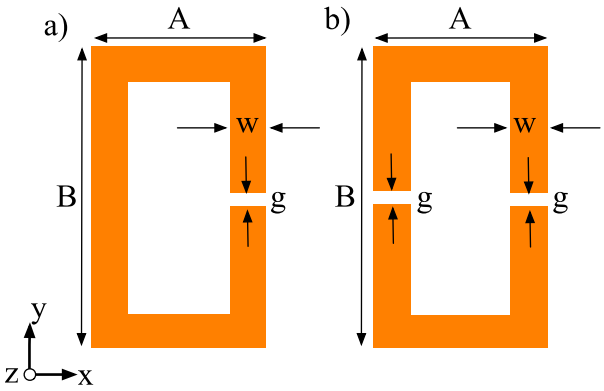

FIG. 1. The schematic of the proposed device.

results of device characterization in section III. We discuss the results in section IV and conclude the studies in Section V.

II. STRUCTURE AND DESIGN OF THE RESONATORS

The device is composed of a 35 μm-thick metallic rectangular loop on a 0.8 mm thick FR-4 substrate as shown schematically in Figure 1. Two types of devices are defined with a single split (Figure 1(a) and two splits (Figure 1(b). Side A and side B of the outer rectangle are 30 and 60 mm, respectively. The width, w, of the loop is 6 mm and the gap of the split, g, is 2 mm.

We modeled the resonators with different boundary conditions using commercially available electromagnetic simulation software (CST Studio Suite, Darmstadt Germany). First, the wave vector, $\vec{k}$, is aligned with the x-axis (see Figure 1), electric field ($\vec{E}$) and magnetic field ($\vec{H}$) vectors are aligned with the y-axis and the z-axis, respectively. The results of the simulation for the single-split resonator are shown in Figure 2. Magnetic field is perpendicular to the loop, so it supports circulating current along the conductive path. In addition, electric field is polarized along the gap that also contributes a circulating current. The combined effect results in the first resonant frequency, which can be identified as magnetic resonance at 0.65 GHz. The vectors for current density at this frequency are shown in Figure 2(b). The second resonant frequency is observed at 3.28 GHz, which is identified as an electric resonant frequency due to the electric field aligned along the side B of the resonator. The distribution of the electric field at this frequency is shown in Figure 2(c).

In the second setting, $\vec{E}$ is aligned with the x-axis, $\vec{k}$ and $\vec{H}$ are aligned with the y-axis and the z-axis, respectively. The resultant spectrum of *s21* for the single-split resonator is shown in Figure 3(a). In this case, magnetic field is perpendicular to the loop similar to the previous setting. This results in a resonant behavior that supports a circulating current along the conducting path. Consequently, the first resonant frequency is observed at 0.61 GHz and the current field distribution for this resonance is plotted in Figure 3(b). The first resonant frequency for this setting is almost the same with the one for the first setting. However, the electric field is now along the x-axis and is polarized along the side A of the resonator. This supports a certain circulating current pattern as will be explained for the third setting (see Figure 4). The magnetic resonance is induced due to the combinatory effect of the electric and the magnetic field. The resonant frequency is 1.14 GHz, for which a density of current vectors as shown in Figure 3(c). So, changing the polarization of the electric field and the propagation vector results in an additional magnetic resonance. The third resonant frequency is due to electric resonance at 3.73 GHz. At this frequency, the electric field is aligned along with the side A of the resonator as shown in Figure 3(b).

In the third setting, $\vec{E}$ is aligned with the x-axis, $\vec{H}$ and $\vec{k}$ are aligned with the y-axis and the z-axis, respectively. The results of the simulation for the single-split resonator are shown in Figure 4. Unlike the previous settings, the magnetic field is not perpendicular to the loop. Thus, a circulating current stemming from the magnetic field is not expected in this case. However, the

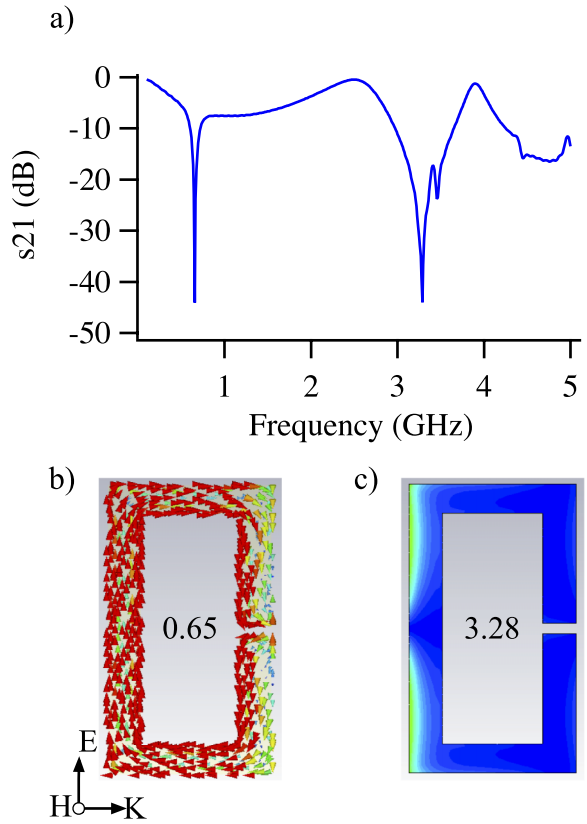

FIG. 2. a) s21 spectrum of the single-split resonator for the excitation setting shown in the figure. b) Distribution of the current density at the first resonant frequency of 0.65 GHz. c) Distribution of the electric field at the second resonant frequency of 3.28 GHz.

electric field is polarized along the side *A* of the device. Left and right hand sides of the structure are polarized with opposite charges at resonance and the presence of the split defines a symmetry axis along the x-axis through the split. This results in two identical circulating current loops in opposite directions in the upper and lower halves of the resonator as shown in Figure 4(b). The rectangular shape of the resonator and relatively short length of side *A* support the circulation of the current paths shown in Figure 4(b). The lengths of the current loops are shorter as compared to the previous cases. Thus, the resonant frequency for the magnetic resonance is higher at 1.86 GHz. The second resonant frequency of 4.73 GHz is due to the electric resonance as a result of electric field along with the side *A* of the resonator.

In the forth setting, $\vec{H}$ is aligned with the x-axis, $\vec{E}$ and $\vec{k}$ are aligned with the y-axis and the z-axis, respectively. The results of the simulation for a single-split resonator are shown in Figure 5. Similar to the third setting, the magnetic field is not perpendicular to the device. So, circulating current along the loop is not expected due to the magnetic field. However, the electric field is polarized along the split, inducing a single path of circulating current in the loop. The resonant frequency of this magnetic resonance is 0.81 GHz for which the distribution of current vectors is shown in Figure 5(b). The first resonant frequency is 25% larger than the one obtained for the case of magnetic field that is perpendicular to the loop (the first and the second settings), because of the smaller length of the equivalent conductor path as observed in Figure 5(b). The second and the third resonant frequencies are due to electric resonances. The distributions of the electric field for the electric resonances are shown in Figure 5(c)-5(d).

All the simulation results obtained for the single-split resonator under different excitations are summarized in Table I. The orientation for *E*, *H* and *k* vectors are defined with respect to the coordinate axes and device orientation defined in Figure 1.

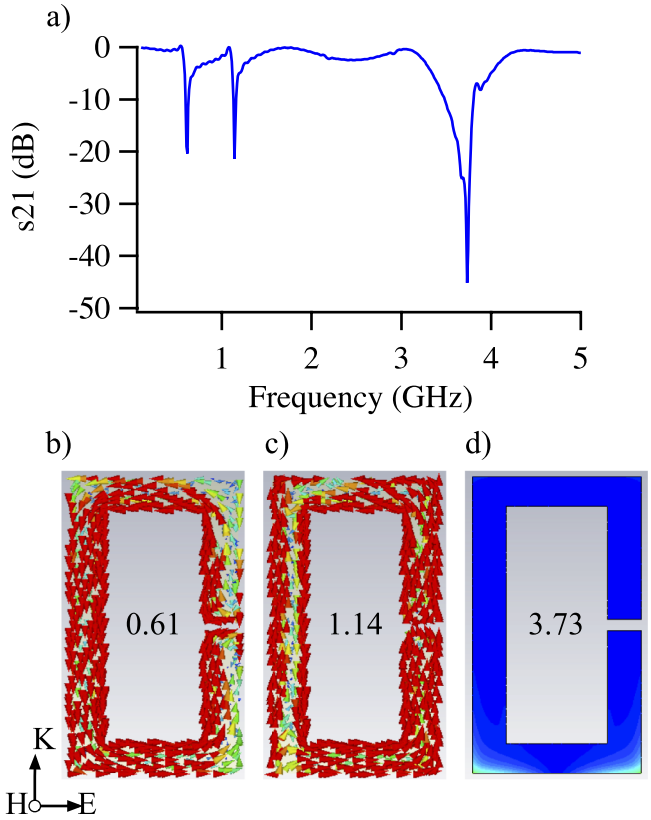

FIG. 3. a) s21 spectrum of the single-split resonator for the excitation setting shown in the figure. Distribution of current densities at b) the first resonant frequency of 0.61 GHz, c) at the second resonant frequency of 1.14 GHz. d) Distribution of electric field at the third resonant frequency of 3.73 GHz.

Figure 6 shows the dependency of the resonant behavior to the orientation of the electric field. Inset to the Figure 6, we define an angle θ between the electric field and the side B of the resonator. An angle of zero degrees corresponds to the case of fourth setting (see Figure 5) whereas an angle of ninety degrees corresponds to the case of third setting (see Figre 4). The first and the second resonant frequencies shown in Figure 6 correspond to the magnetic resonances as explained before. The third resonant frequency corresponds to the electric resonance. The magnetic resonances are induced based on the presence of the electric field vector along the x-axis and the y-axis (see Figure 1). For the extreme angles of zero and ninety, the electric field is aligned either along the y-axis or the x-axis. So, only one of the magnetic resonances is excited. On the other hand, for an oblique angle, the electric field has components on both axes that results in magnetic resonance at both frequencies. The resonant frequencies for magnetic resonances are the same for different orientations of the incident. We have observed a slight variation in the second resonant frequency due to a change in the conduction path that is determined by the electric field vector along the x-axis. On the other hand, the electric resonant frequency is varying with the angle as observed in Figure 6. The frequency shifts with the effective conductor length along the direction of electric field vector. The effective conductor length is the shortest for the angle of zero and this corresponds to the largest resonant frequency.

In the fifth setting, two-splits resonator (see Figure 1(b)) was simulated. The resultant spectrum of *s21* for the two-splits resonator is shown in Figure 7(a) for a case where $\vec{E}$ is aligned with the x-axis while $\vec{H}$ and $\vec{k}$ are aligned with the y-axis and the z-axis, respectively. The magnetic field is not perpendicular to the resonator, preventing the occurrence of magnetic resonance due to a circulating current. On the other hand, the electric field is along with the side A of the device. The settings of the field vectors are the same with the third case presented in Figure 4. The first resonant

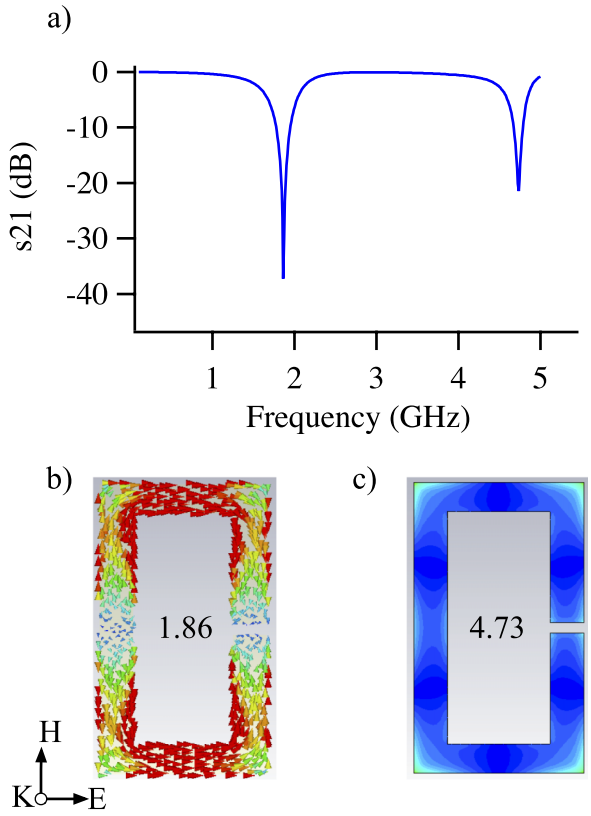

FIG. 4. a) s21 spectrum of the single-split resonator for the excitation setting shown in the figure. b) Distribution of current density at the first resonant frequency of 1.86 GHz c) Distribution of electric field at the second resonant frequency of 4.73 GHz.

frequency is at 1.87 GHz and the resultant distribution of current vectors is shown in Figure 7(b). The frequency and the distribution of current vectors are identical with the results presented in Figure 4. It is surprising to observe an identical response for a two-splits device as compared to a single-split one considering the first resonant frequency. The resonators are functionally identical considering the electric field polarization. The electric field supports two paths of circulating current in opposite directions in bottom and top halves of both resonators. Hence, two virtual nodes are defined along the x-axis passing through the split, regardless of the number of splits as verified in Figure 4(b) and Figure 7(b).

III. EXPERIMENTAL CHARACTERIZATION

We fabricated the resonators on an FR4 substrate with a thickness of 0.8 mm utilizing standard printing circuit board manufacturing techniques. The thickness of the metal lines is 35 μm. We used a pair of monopole patch antennas with a length of 30 mm and a width of 3.5 mm to excite the resonators. The distance between two antennas is 10 cm. We placed the resonators and the antennas on an aluminum back plate that we used as a ground plane. We connected the antennas to a vector network analyzer (Rohde and Schwarz, Munich, Germany) to obtain the transmission parameters. The setup is shown in Figure 8. In this orientation, the propagation vector, k, is along the short sides of the rectangle as shown in the figure.

The antennas have omnidirectional radiation pattern. Therefore, the location and the orientation of the resonators between the antennas can be adjusted to excite the resonators in a desired setting. Figure 9 shows the spectrum of s21 for the single-split resonator in a certain configuration where the excitation is the same with the case explained in Figure 5. The simulated s21 spectrum of Figure 5 is

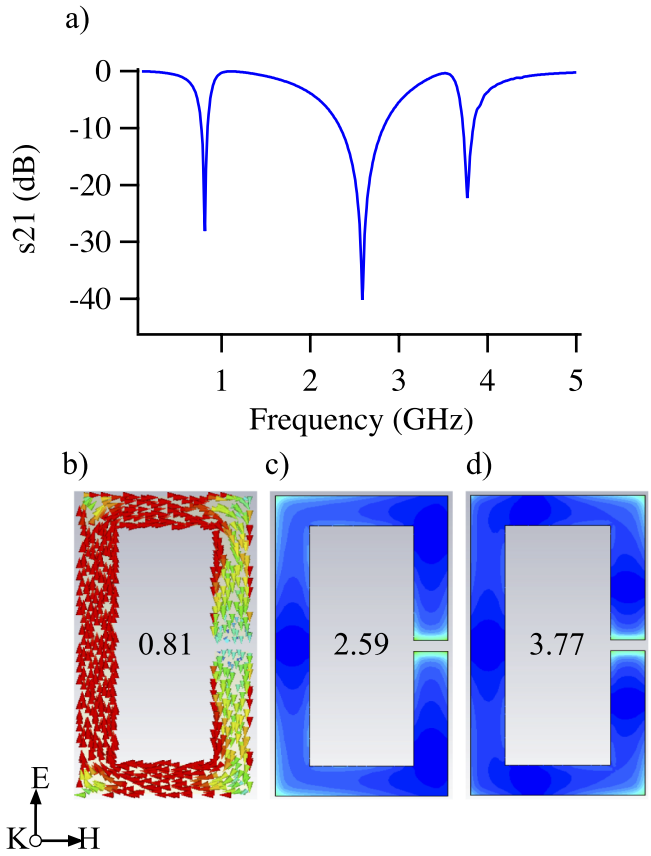

FIG. 5. a) s21 spectrum of the single-split resonator for the excitation setting shown in the figure. b) Distribution of current density at the first resonant frequency of 0.81 GHz. Distributions of electric field at c) the second resonant frequency of 2.59 GHZ and d) at 3.77 GHz.

also plotted in Figure 9 for convenience. The measured values of the resonant frequencies are 0.82 GHz, 2.1 GHz and 4.29 GHz. The first resonant frequency is due to the magnetic resonance because of the electric field that is polarized along the gap of the device. The measured value is 1% larger than the simulation result. The second and the third resonant frequencies are due to the electric resonance as explained before. The measured value for the second resonant frequency is smaller than the simulation result by 19%, whereas the measured value for the third resonant frequency is higher than the simulation result by 14%.

Then, we changed the orientation of the single-split resonator to have the electric field aligned with side *A* similar to the case explained in Figure 4. Figure 10 shows the spectrum of s21 in this configuration. The simulated s21 spectrum of Figure 4 is also plotted in Figure 10 for convenience. We observed a single resonance within 0-4 GHz range at 2.14 GHz. This corresponds to the magnetic resonance due to the electric field along side *A*. The measured value of the resonant frequency is larger than the simulation result by 15%.

TABLE I. Summary of Simulation Results under Different Excitations.

Orientation	1st resonant frequency	2nd resonant frequency	3rd resonant frequency	Corresponding Figure
k:x, E:y, H:z	0.65 GHz	3.28 GHz	-	Figure 2
E:x, k:y, H:z	0.61 GHz	1.14 GHz	3.73 GHz	Figure 3
E:x, H:y, k:z	1.86 GHz	4.73 GHz	-	Figure 4
H:x, E:y, k:z	0.81 GHz	2.59 GHz	3.77 GHz	Figure 5

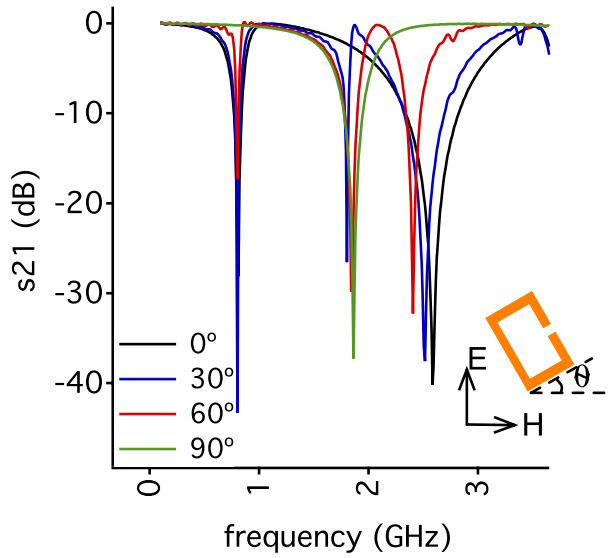

FIG. 6. s21 spectra of the single-split resonator for different orientations of the electric field.

We repeated this measurement configuration for the two-splits resonator and observed a very similar spectrum of s21 as compared to the single-split device of Figure 10. The spectrum is shown in Figure 11 with a single resonance at 2.12 GHz. This value is larger than the simulation result of Figure 7 by 13%. The simulated s21 spectrum of Figure 7 is also plotted in Figure 11 for

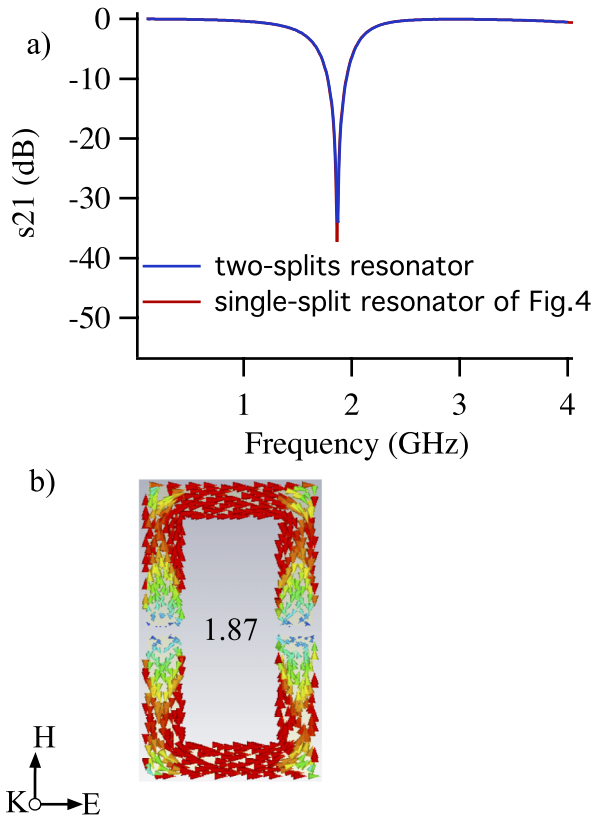

FIG. 7. a) s21 spectrum of the two-splits resonator for the excitation setting shown in the figure, compared to that of Figure 4. b) Distribution of current density at the first resonant frequency of 1.87 GHz.

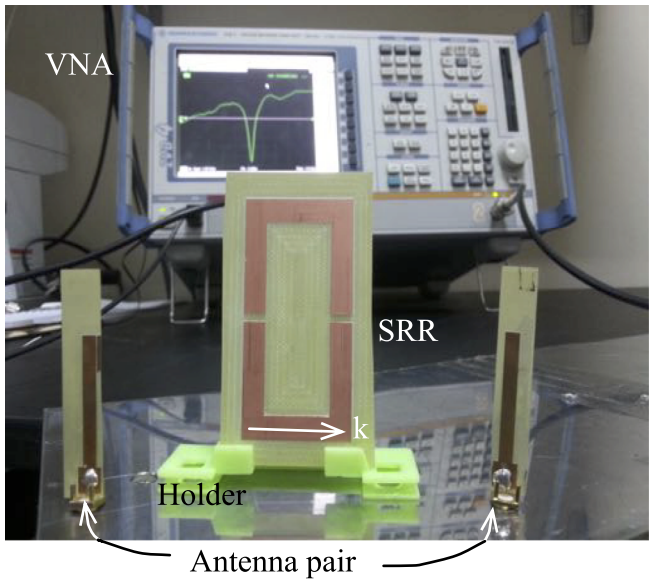

FIG. 8. The experimental setup.

convenience. The experimental results verify the resonance behavior of the single-split and two-splits resonators are the same for the specific excitation configuration shown in Figure 4 and 7.

IV. DISCUSSION

An important conclusion of this paper as mentioned previously is that the two-split and one-split rectangular rings can have identical behaviors under specific E field polarization. It can be inferred from Figure 4 and Figure 7 that electric field generates two circulating current paths on

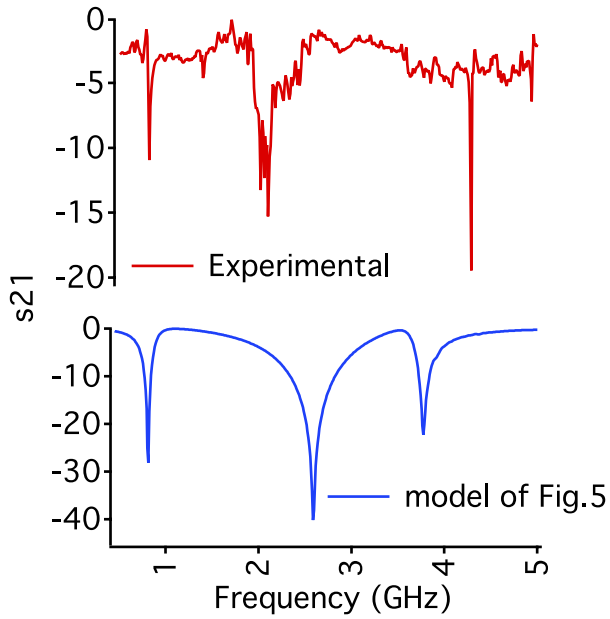

FIG. 9. Spectrum of s21 for a single-split resonator in an excitation setting similar to that of Figure 5. The measured values of resonant frequencies are 0.82 GHz, 2.1 GHz and 4.29 GHz.

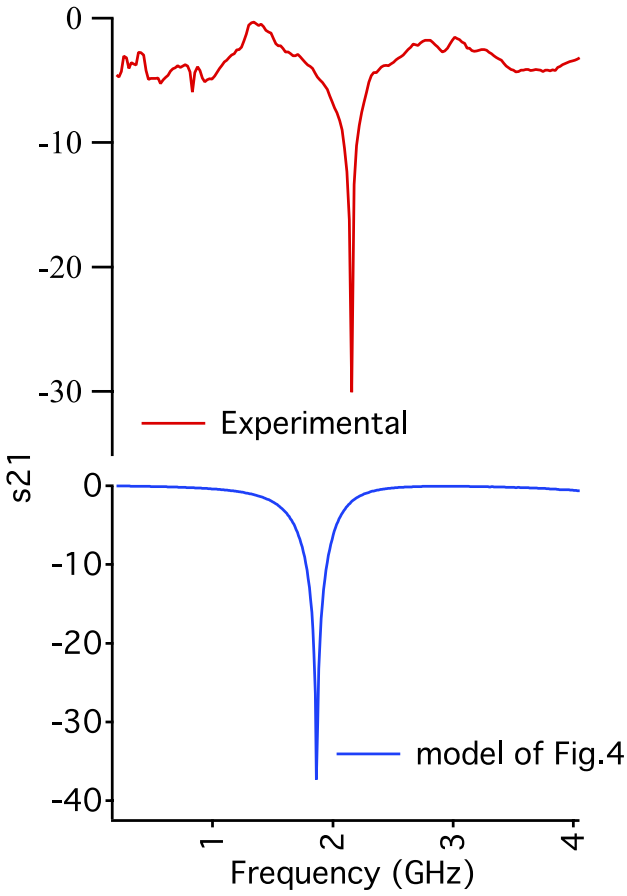

FIG. 10. Spectrum of s21 for a single-split resonator in an excitation setting similar to that of Figure 4. The measured value of resonant frequency is 2.14 GHz.

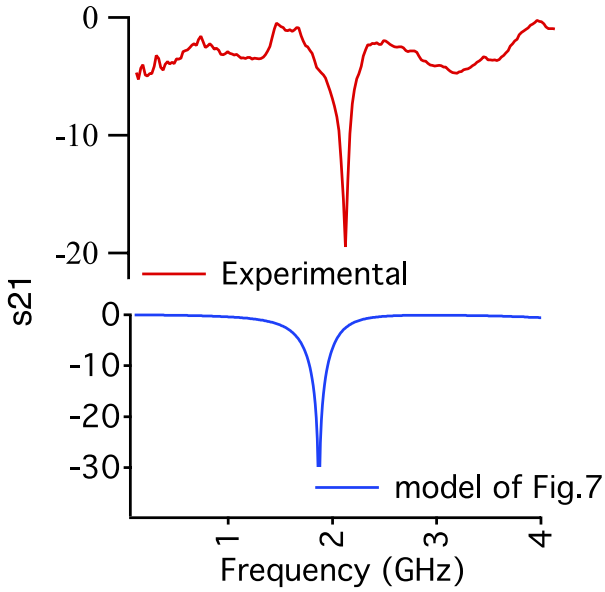

FIG. 11. Spectrum of s21 for a two-splits resonator in an excitation setting similar to that of Figure 7. The measured value of resonant frequency is 2.12 GHz.

top and bottom halves of the rings and thus generating two virtual nodes on long sides (side B, see Figure 1) of each rectangle. So, the first resonant frequency, which is due to magnetic resonance, is the same for both devices regardless of the number of splits. We presented the experimental characteristics of these devices in Figure 10 and Figure 11 that show the experimental results are in a good agreement with simulation results.

The discrepancies between resonant frequencies in experimental results and simulation results vary from 1% in the case of magnetic resonant frequencies to 19% in the case of second electric resonance in Figure 9. The possible sources of errors include the possibility of slight geometrical differences between the fabricated rings and the simulated ones. Specifically, differences in the effective path length shown in Figure 5(c) and 5(d) between the simulated and experimentally characterized devices can result in a discrepancy between electric resonances as observed in Figure 9.

We have used monopole antennas since they allow us to control different excitations in a single setup by manipulating the position of the devices. Also, we can effectively couple these compact antennas with the devices. However, because of omnidirectional radiation paths of these antennas, it is difficult to have control in a very strict sense over the orientations of E and H fields and this contributes to the minor divergence between the simulation and experimental results. In addition, we have observed that the resonant dips in simulations are generally sharper than the ones in experimental results indicating that the fabricated rings are lossier than the models used in simulation settings.

V. CONCLUSION

In summary, we present modeling and experimental characterization results for rectangular split-ring resonators with a single split and two-splits that operate at microwave frequencies between 1 and 5 GHz. Different excitation conditions are imposed on the resonators that result in different resonance behavior. The orientation of the electric and the magnetic field determines the resonant mode and the frequency as explained with electromagnetic simulations. We observe magnetic resonance as a result of magnetic field perpendicular to the plane of the resonator. This induces a circulating current pattern along the conductor of the resonator. A similar current pattern is obtained when the electric field is polarized along with the gap of the resonator. We also observe a different mode of magnetic resonance when the electric field is along with the short side of the resonator. In this case, two different current paths with opposing current directions are present in bottom and top halves of the resonator. The rectangular shape of the resonators supports this mode of operation where two virtual nodes are defined along the gap of the resonator. We show that the presence of the node and the paths of circulating current are the same for the two-splits resonator with identical excitation conditions. We place the second split of the resonator exactly at the second node so that the circulating current path is not altered. So, the magnetic resonance behavior of the resonators is the same regardless of the splits on the structure for a certain excitation condition. We fabricated the resonators on an FR4 substrate for experimental characterization and used a pair of monopole antennas to excite the resonators. We verify the results of the simulations with the experiments. The results are in good agreement with a maximum deviation of 19% between the values of resonant frequencies. Experimental results show that the presented devices can effectively function as frequency selective media for varying excitation conditions.

ACKNOWLEDGMENTS

This work is supported by the Tübitak Grant No. 112E250.

[1] Vladimir M Shalaev, Nature Photonics **1**, 41-48 (2007).
[2] R A Shelby, D R Smith, and S Schultz, Science **292**, 77-9 (2001).
[3] John B Pendry, A J_ Holden, D J Robbins, and W J Stewart, "Microwave Theory and Techniques," IEEE Transactions on **47**, 2075-2084 (1999).
[4] Costas M Soukoulis, Stefan Linden, and Martin Wegener, Science **315**, 47-49 (2007).
[5] J B Pendry, D Schurig, and D R Smith, Science **312**, 1780-2 (2006).

[6] David Schurig, J J Mock, B J Justice, Steven A Cummer, John B Pendry, A F Starr, and D R Smith, Science **314**, 977-980 (2006).
[7] Pendry, Phys Rev Lett **85**, 3966-9 (2000).
[8] Igor I Smolyaninov, Yu-Ju Hung, and Christopher C Davis, Science **315**, 1699-701 (2007).
[9] Zhaowei Liu, Hyesog Lee, Yi Xiong, Cheng Sun, and Xiang Zhang, Science **315**, 1686 (2007).
[10] Vikrant Jayant Gokhale, Olga Shenderova, Gary E McGuire, and Mina Rais-Zadeh, Microelectromechanical Systems, Journal of **23**, 191-197 (2014).
[11] J T Hong, D J Park, J H Yim, J K Park, Ji-Yong Park, Soonil Lee, and Y H Ahn, The Journal of Physical Chemistry Letters **4**, 3950-3957 (2013).
[12] Tao Chen, Suyan Li, and Hui Sun, Sensors (Basel) **12**, 2742-65 (2012).
[13] Yun-Tzu Chang, Yueh-Chun Lai, Chung-Tien Li, Cheng-Kuang Chen, and Ta-Jen Yen, Optics Express **18**, 9561-9569 (2010).
[14] H Torun, F Cagri Top, G Dundar, and A D Yalcinkaya, Journal of Applied Physics **116**, 124701 (2014).
[15] S J Park, J T Hong, S J Choi, H S Kim, W K Park, S T Han, J Y Park, S Lee, D S Kim, and Y H Ahn, Sci Rep **4**, 4988 (2014).
[16] Christian Debus and Peter Haring Bolivar, Applied Physics Letters **91**, 184102 (2007).
[17] David R Smith, John B Pendry, and Mike CK Wiltshire, Science **305**, 788-792 (2004).
[18] O Sydoruk, E Tatartschuk, E Shamonina, and L Solymar, Journal of Applied Physics **105**, 014903 (2009).
[19] Ibraheem A Ibraheem Al-Naib, Christian Jansen, and Martin Koch, Applied Physics Letters **93**, 083507 (2008).
[20] M Kafesaki, Th Koschny, R S Penciu, T F Gundogdu, E N Economou, and C M Soukoulis, Journal of Optics A: Pure and Applied Optics **7**, S12 (2005).
[21] R S Penciu, K Aydin, M Kafesaki, Th Koschny, E Ozbay, E N Economou, and C M Soukoulis, Optics Express **16**, 18131-18144 (2008).
[22] Koray Aydin, Irfan Bulu, Kaan Guven, Maria Kafesaki, Costas M Soukoulis, and Ekmel Ozbay, New Journal of Physics **7**, 168 (2005).